Korean J. Chem. Eng., **27**(1), 96-103 (2010)
DOI: 10.1007/s11814-009-0315-3

Prediction of thickness and fouling rate in pulsating flow heat exchangers, using FLUENT simulator

Nasser Saghatoleslami*,†, Mehdi Koolivand Salooki*, and Mohammad Ali Armin**

*Department of Chemical Engineering, Ferdowsi University of Mashhad, Mashhad, Iran
**Department of Chemical Engineering, Shahrood Azad University, Shahrood, Iran
(*Received 18 April 2009 • accepted 24 June 2009*)

Abstract−Heat exchangers are an important part of industrial processes as they handle a major portion of total energy consumption. Fouling could have serious impact on their performance and hence affect the economic performance of the process plant. The aim of this work was to simulate the crystallization fouling process in a heat exchanger by developing a C^{++} program and adopting UDF functions through Fluent software; and hence evaluate all the given models and consequently implement the model which would best suit our particular case. The finding of this work would enable us to evaluate the thickness and fouling rate in the heat exchangers. Furthermore, the effect of pulsating flow on the crystallization fouling of calcium sulfate ($CaSO_4$) in the heat exchanger was also investigated, and the effect of operation of different amplitude of the oscillations (10-70) and frequencies (1.59-12.73 Hz) on the fouling of this compound was studied.

Key words: Fouling, Heat Exchanger, Pulsating Flow, Fouling Resistance, Calcium Sulfate

INTRODUCTION

There are many engineering practical situations where heat is being transferred under conditions of pulsating and reciprocating flows such as the operation of modern power producing facilities and industrial equipment used in metallurgy, aviation, chemical and food technology. Cavitations in hydraulic pipelines, pressure surges and flow of blood are also some familiar instances of such flows. The performance of this equipment in thermal engineering applications is affected by the pulsating flow parameters [1]; during the past few decades, numerous studies have been devoted to this pulsating flow and its associated heat transfer problems.

The pulsating flow effects could be beneficial in many applications. Examples are extraction pulsating columns [2], pulsed combustor for both civil and military uses, reciprocating engines, ramjet and cooling systems for nuclear reactors [3]. Several studies with conflicting results were carried out on the effect of the oscillatory motion of the flow on mass and heat transfer [2,4,5]. Brunold [6] showed that pulsating flows could promote chaotic mixing in a tube, in which radial velocity components are significant. Gbadebo [8] found that heat transfer could be enhanced at medium frequencies of pulsation and reduced at both higher and lower frequencies within their experimental ranges. Pérez [9] analyzed mass and momentum transfer in an annular electrodialysis cell involving laminar oscillating flow. They found that pulsating flow allows enhancing mass transfer due to the increase of the local velocity gradient at the surface. These authors also showed that the increase in turbulence level by flow pulsation plays a relevant role in convective mass and heat transfer between a solid wall and a liquid. On the other hand, Martinelli [10] experimentally studied heat transfer, and reported that the frequency has no direct effect on the Nusselt number. Mao and coworkers in 1985 found that imposed oscillations on a turbulent flow had no effect on the time-mean velocity gradient at the wall [11,12]. However, only small amplitudes of imposed oscillations were used in their experiments. Thus, the variety of results found in the literature seems to be related to the type of pulsation generator and to the mean flow rate used during experiments. Unfortunately, in many papers, some important parameters were not considered, especially the amplitude of the oscillations [1,8].

The aim of this work was to simulate the crystallization fouling process in a heat exchanger by developing a C^{++} program and adopting UDF functions through Fluent software; and hence to evaluate all the given models and consequently implement the model which would best suit our particular case. Furthermore, numerically investigate the effect of pulsation frequency as well as the amplitude of the oscillations on the fouling of plate heat exchanger characteristics of turbulent pulsating flow over a range of the frequency (1.59-12.73 Hz) and amplitude of the oscillations (10-70).

COMPUTATIONAL PROCEDURES

1. Numerical Methods

The numerical simulations are performed by solving the time-dependent, continuity, momentum and energy equations for an incompressible fluid in the 2D flat plate. In dimensionless form, these equations are:

$$\frac{\partial u}{\partial x}+\frac{\partial v}{\partial y}=0 \tag{1}$$

$$\frac{\partial u}{\partial t}+u\frac{\partial u}{\partial x}+v\frac{\partial u}{\partial y}=-\frac{\partial P}{\partial x}+\frac{1}{Re}\left[\mu\left(\frac{\partial^2 u}{\partial x^2}+\frac{\partial^2 v}{\partial y^2}\right)+2\frac{\partial \mu}{\partial x}\frac{\partial u}{\partial x}+\frac{\partial \mu}{\partial y}\left(\frac{\partial u}{\partial y}+\frac{\partial v}{\partial x}\right)\right] \tag{2}$$

†To whom correspondence should be addressed.
E-mail: slami@um.ac.ir

$$\frac{\partial v}{\partial t}+u\frac{\partial v}{\partial x}+v\frac{\partial v}{\partial y}=-\frac{\partial P}{\partial y}$$
$$+\frac{1}{Re}\left[\mu\left(\frac{\partial^2 v}{\partial x^2}+\frac{\partial^2 v}{\partial y^2}\right)+2\frac{\partial\mu}{\partial y}\frac{\partial v}{\partial y}+\frac{\partial\mu}{\partial x}\left(\frac{\partial u}{\partial y}+\frac{\partial v}{\partial x}\right)\right] \quad (3)$$

$$\frac{\partial T}{\partial t}+u\frac{\partial T}{\partial x}+v\frac{\partial T}{\partial y}=\frac{1}{RePr}\left[k\left(\frac{\partial^2 T}{\partial x^2}+\frac{\partial^2 T}{\partial y^2}\right)+\frac{\partial k}{\partial x}\frac{\partial T}{\partial x}+\frac{\partial k}{\partial y}\frac{\partial T}{\partial y}\right] \quad (4)$$

Simulations are performed on a staggered grid with a finite volume method. All terms, including convective fluxes, are discretized using second-order central differencing, and a low storage third order Runge-Kutta algorithm is used for time integration. The continuity equation and the pressure gradient term in the momentum equations are treated implicitly, while the convective and diffusive terms are treated explicitly. A preconditioned conjugate gradient solver is used for matrix computation. Temperature variations are assumed to be small enough so that fluid properties can be considered constant resulting the decoupling of the hydrodynamics equations from the energy transport equation. Accordingly, the energy equation is solved explicitly after the hydrodynamics have been computed.

2. Fouling Formulation

The temperature along the heat transfer surface would enable the calculation of the deposition and removal rates, i.e., the deposit that was accumulated or removed from unit area per unit time from the fouling layer. The total mass rate is defined as a difference between deposition and removal mass rates:

$$\frac{dm}{dt}=\frac{dm_d}{dt}-\frac{dm_r}{dt}\Rightarrow \dot{m}=\dot{m}_d-\dot{m}_r \quad (5)$$

The crystal mass per surface area at a determined time t+Δt is calculated as a sum of the total mass per surface area at time added to the calculated mass rate during the new computing time step Δt:

$$m_{t+\Delta t}=m_t+\frac{dm}{dt}\cdot\Delta t=m_t+\dot{m}\cdot\Delta t \quad (6)$$

In all the computation, the time step was set as Δt=1 h. The thickness of the fouling layer is then calculated as the total deposit mass per surface area divided by the density ρ_f of the fouling layer:

$$x_f=\frac{m_{t+\Delta t}}{\rho_f} \quad (7)$$

DEPOSITION MASS RATE MODEL

It was assumed that all ions of calcium sulfate transported to the phase boundary would participate in the surface reaction. The equations for the calculation of the transported and inserted mass rates could then be combined by eliminating the unknown concentration c_f at the phase boundary. The combination leads to a relationship for the calculation of the deposition mass rate that considers the mass transfer resistance [14,18]:

$$\dot{m}_d=\beta\left[\frac{1}{2}\frac{\beta}{k_R}+\Delta c-\left(\frac{1}{4}\left(\frac{\beta}{k_R}\right)^2+\frac{\beta}{k_R}\cdot\Delta c\right)^2\right] \quad (8)$$

where c_S is the saturation concentration and is calculated as a function of T_f at the phase boundary [16]:

Table 1. Model coefficients for the calculation of the saturation concentration [16]

	$CaSO_4$
a_1	−44550.53
a_2	−183.04
a_3	61.83

Table 2. Model coefficients for the calculation of the diffusion coefficient [16]

b_1	b_2	b_3	b_4
3.923e-16	2.333e-15	7.153e-12	1.049e-10
b_5	b_6	b_7	b_8
-2.539e-16	1.087e-13	1.036e-11	2.769e-10

$$\log(c_S)=-\frac{a_1}{2\cdot 3\cdot R\cdot T_f}+\frac{a_2}{R}\cdot\log(T_f)+a_3 \quad (9)$$

The coefficients in Eq. (9) are shown in Table 1 [16].

For the determination of the diffusion coefficient of calcium sulfate in aqueous solution, a computing model based on calculation results of Lammers was developed [16]. This model describes the dependency of the diffusion coefficient on the two parameters of temperature and concentration as:

$$D(T,c)=\frac{b_1\cdot T^3+b_2\cdot T^2+b_3\cdot T+b_4}{c+1}+b_5\cdot T^3+b_6\cdot T^2+b_7\cdot T+b_8 \quad (10)$$

The coefficients in Eq. (10) are shown in Table 2 [16].

The mass transfer coefficient could be determined as a function of the Sherwood number and the diffusion coefficient as:

$$\beta=\frac{Sh\cdot D}{d_h} \quad (11)$$

For the calculation of the Sherwood number, a semi-empirical approach according to Lammers was adopted [16]:

$$Sh=0.034\cdot Re^{0.875}\cdot Sc^{1/3} \quad (12)$$

DENSITY OF THE FOULING LAYER

The density of the fouling layer is one of the most important quantities for the calculation of the fouling resistance. It not only affects the calculation of the removal mass rate but also the calculation of the layer thickness itself. A cross section of a fouling layer shows that the layer is not homogeneous. In most cases four layers could be differentiated, which are different in the structure, color and strength [17].

Hirsch [17] noticed that the density of the fouling layer depends not only on the local position in the layer but also on the total thickness of the crystal layer. For the numerical simulation, it was necessary to calculate both unsteady and local values of the density of the fouling layer because of the relationship between time and the calculated total thickness of the crystal layer (Fig. 1).

Based on results of abrasion experiments and by neglecting the aging effect of the crystal layer, the following computer model was

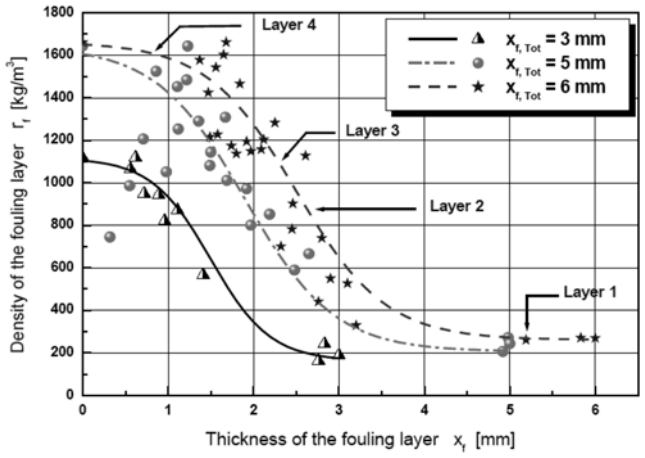

Fig. 1. Local density ρ_f versus total thickness of the fouling layer [17].

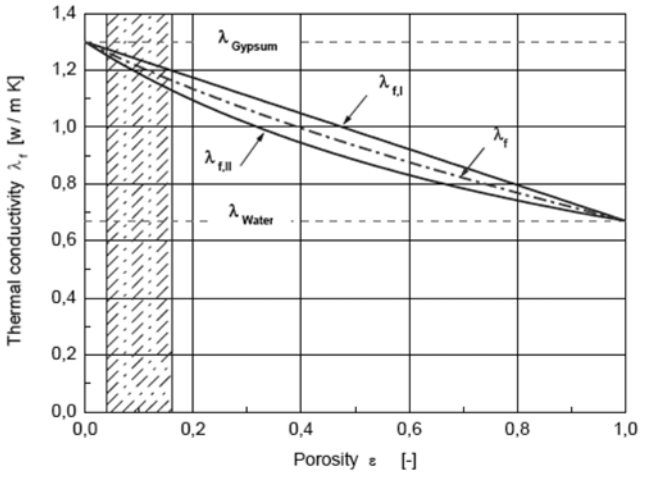

Fig. 2. Thermal conductivity λf versus porosity of the fouling layer [18].

Table 3. Model coefficients for the calculation of the density of the fouling layer [14,17]

c_1	$10^3 \cdot \log(1.11+0.7 \cdot x_{f,Tot})$
c_2	$105+22.5 \cdot x_{f,Tot}$
c_3	$0.5 \cdot x_{f,Tot}$
c_4	$0.25 \cdot x_{f,Tot}$

developed and integrated into the numerical simulation by Augustin [14,17]. It describes a unique relationship between the density of the fouling layer ρ_f and the two parameters; local position within the fouling layer x_f and total thickness of the fouling layer $x_{f,Tot}$.

$$\rho_f(x_f, x_{f,Tot}) = c_2 + \frac{c_1 - c_2}{1+10^{\left(\frac{x_f - c_3}{c_4}\right)}} \tag{13}$$

The coefficients in Eq. (13) are shown in Table 3 [14,17].

REMOVAL MASS RATE

For the calculation of the removal mass rate, the following approach was used [14,18]:

$$\dot{m}_r = \frac{K}{P} \cdot \rho_f \cdot (1+\delta \cdot \Delta T) \cdot d_p \cdot (\rho^2 \cdot \eta \cdot g)^{1/3} \cdot x_f \cdot w^2 \tag{14}$$

where w is the local value of the flow velocity above the crystal layer. P describes the intercrystalline adhesion forces. K is a parameter that is equal to the number of fault points in the fouling layer and describes the temperature stresses in the fouling layer. $(1+\delta \Delta T)$, δ is the linear expansion coefficient and ΔT the temperature gradient in the fouling layer d_p is the mean crystal diameter.

HEAT TRANSFER

The thermal conductivity could be calculated based on measurement results of the porosity of the fouling layer. It was computed by the thermal conductivity of the pore medium (λ_{Water}=0.67 W/mK) and the compact solid (λ_{Gypsum}=1.3 W/mK). After considerations of Krischer [18] over the thermal conductivity of porous systems, two limit curves for the thermal conductivity of the material system gypsum/water for parallel joined resistances were represented through:

$$\lambda_{f,I} = \varepsilon \cdot \lambda_{Water} + (1=\varepsilon) \cdot \lambda_{Gipsum} \tag{15}$$

and accordingly for in series connected resistances through:

$$1/\lambda_{f,II} = \varepsilon/\lambda_{Water} + (1-\varepsilon)/\lambda_{Gipsum} \tag{16}$$

The thermal conductivity of the fouling layer is then computed as the arithmetic average value of both limit values:

$$\lambda_f = (\lambda_{f,I} + \lambda_{f,II})/2 \tag{17}$$

The graphical evaluations of Eqs. (15) and (16) for the entire porosity range ε are represented in Fig. 2. The mean values according to the dash-dotted lines approximate the thermal conductivity of the porous fouling layer in accordance with Eq. (17). The measured porosity range, in Fig. 2 represented as a hatched area, lies between 5 and 15% [18]. On the average a mean porosity of $\bar{\varepsilon}$=10% was measured. It follows that:

$$\lambda_f = 1.2 \text{ W/m·K} \tag{18}$$

The results revealed that the computation of temperature distributions along the heat transfer surface and/or phase boundary crystal layer/salt solution rises continuously in flow direction. This led again to a not realistic calculation of the fouling layer thickness distribution. The numerical simulation supplies an unrealistic profile of the fouling layer. In reality, the heat flows through the section of the fouling layer with the smallest thermal resistance. Therefore, a local and unsteady heat flux distribution along the heat transfer surface is formed (Fig. 3). The maximal heat flux $\dot{q}_{max}$ would flow through the wall cell with the thinnest crystal layer. Through each other cell flows, a heat flux $\dot{q}_i$ could be calculated as follows:

$$\dot{q}_i = \frac{x_{f,min}}{x_{f,i}} \cdot \frac{\sum_{i=1}^{n} \frac{x_{f,min}}{x_{f,i}}}{n \cdot \dot{q}_o} \tag{19}$$

Eq. (19) states that the larger the layer thickness $x_{f,i}$ above the wall cell, the smaller the heat flux $\dot{q}_i$ that flows through it. Visual observa-

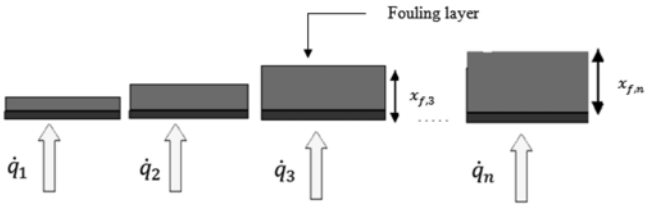

Fig. 3. Principle of the realistic distribution of the heat flux along the heat transfer surface [14].

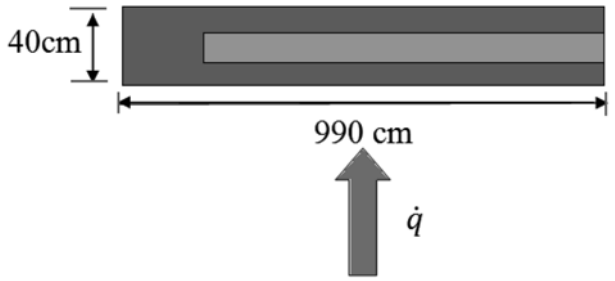

Fig. 4. Computational domain of the case study [14].

tion of the fouling layer shows a local distribution of the thickness along the heat transfer surface, as shown in Fig. 3 [14].

COMPUTATIONAL DOMAIN AND BOUNDARY CONDITIONS

Eqs. (1) to (4) are solved in the computational domain and geometrical flow model as Figs. 4 and 5, respectively, which are subjected to the following boundary conditions [14]:

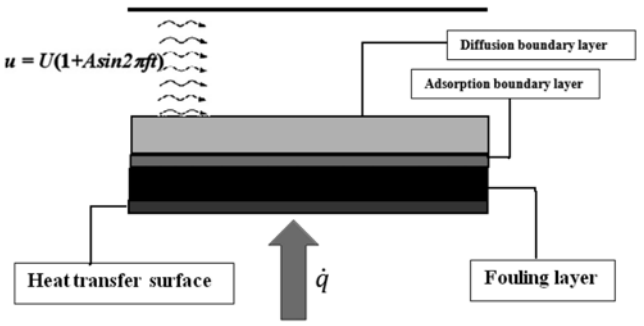

Fig. 5. Geometrical flow model [14].

• Outlet: out flow boundary condition
• Top and bottom: a symmetry condition
• Plate: no-slip condition for velocity and constant heat flux for energy are imposed
• Inlet: free stream pulsating flow in sinusoidal pattern and free stream temperature

The free stream pulsating velocity flow has a sinusoidal pattern, varies with time, and is defined as:

$$u=U(1+A\sin(2\pi ft)) \quad (20)$$

Assumptions:

1. The fluid was constant object property and incompressible fluid
2. Flat plate was laid on horizontal level; the effect of gravitation could be ignored
3. All of the interfaces and contact surfaces were not distorted, fluid-solid contact surface was non-slip boundary
4. The fluid was axisymmetrical two-dimensional flow

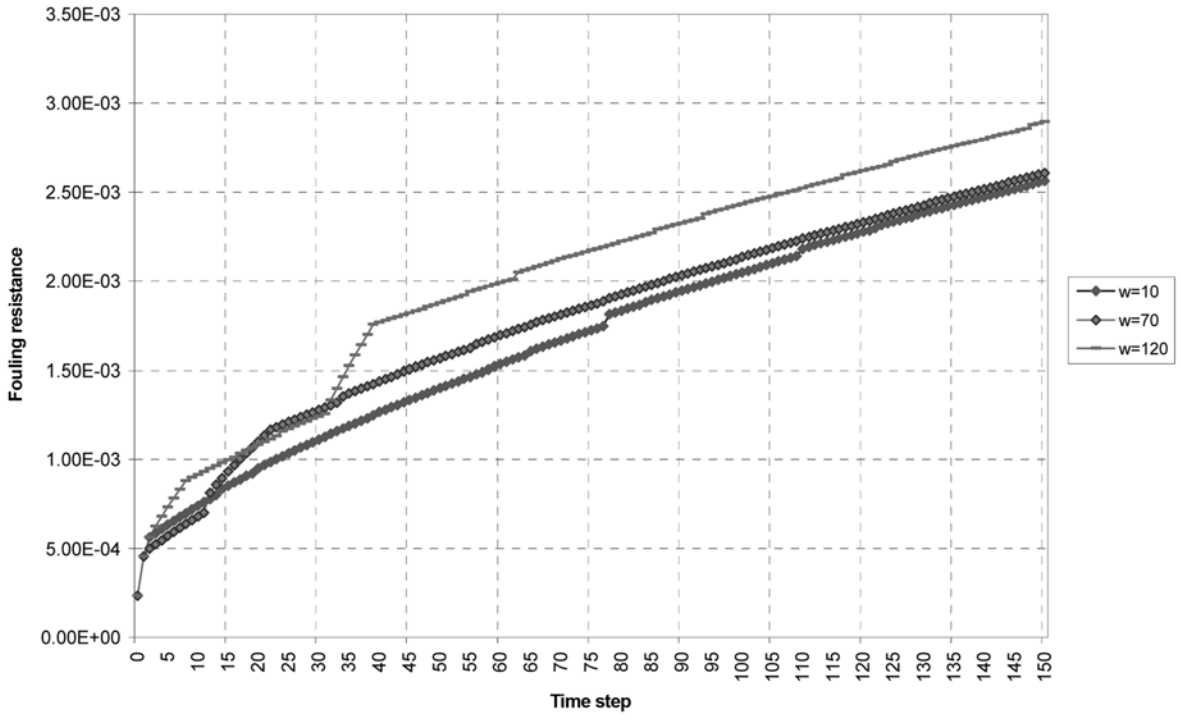

Fig. 6. The effects of variation of angular frequencies on fouling resistance.

SIMULATION, A CASE STUDY

The simulations are performed at moderate frequencies and amplitudes, corresponding to the steady and unsteady transitional regime. For comparative purposes, the mesh size was chosen the same as Brahim and co-workers [14].

RESULTS AND DISCUSSION

1. Effect of Different Frequencies on Fouling Resistances

When the pulse source was located in the upstream, turbulent flow had an influence on the pulsate flow. For a case when u=0.5 m/s, we carried out the numerical calculation of the fouling resistance and fouling thickness under the pulsating turbulence flow pattern in the horizontal channel. As demonstrated in Fig. 6, the amount of the fouling resistance in the pulsate heat exchanger varies with the angular frequency ω. Therefore, for the turbulent region and with an increase in the frequency, the fouling resistance increases accordingly. For the turbulent region, the frequency increases from A=80, f=1.59 Hz (ω=10 rad), $R_{f,t}$ to f=12.73 Hz (ω=120 rad). For this range of frequencies, the fouling thickness increases with frequency in the same trend as the fouling resistance as shown in Fig. 7.

As discussed earlier, there should be a relation between the optimum value of frequency f, fouling resistance, fouling thickness and heat exchanger enhancement. In the case of pulsating flow, the heat effect would be increased and consequently heat transfer efficiency. However, in contrast and in the case of non-pulsating flow, fouling thickness would be greater (Fig. 8). This propagation in fouling resistance causes a reduction in heat transfer efficiency. Therefore, we should select an optimum frequency for the pulsating flow heat exchanger. The findings of this work reveal that for both laminar and turbulent flow, we would approximately have the same optimal frequency [19]. It also shows that both $R_{f,t}$ and $x_{f,t}$ increases with the frequency. Furthermore, oscillation of the velocity and mass flow rate would mainly affect the heat transfer and the temperature gradient in the boundary layer region. If the thermo-resistance in laminar or turbulent sub layer could be diminished, we would be able to enhance the local heat transfer coefficient. If the location of the pulsating source changes, the heat transfer would be completely different with the case where it was in the upstream [19].

2. Effect of Different Amplitude on Fouling Resistances

The variation of the fouling resistance ($R_{f,t}$) and fouling thickness ($x_{f,t}$) in pulsate heat exchanger with the amplitude of oscillation is shown in Figs. 9 and 10.

For the turbulent case, $R_{f,t}$ and $x_{f,t}$ would be increased with a reduction in the frequency amplitude. For the turbulent region, f=11.14 Hz (ω=70 rad), A=10, $R_{f,t}$ increases with the amplitude until A=80. For this range of amplitude, the fouling thickness decreases with amplitude in the same trend as the fouling resistance as shown in Fig. 10.

Pulsation frequency accelerates turbulence fluctuation in the turbulent boundary layer and strengthens momentum and energy conversion and hence increases $x_{f,t}$ and $R_{f,t}$. However, pulsation of amplitude would cause more turbulent fluctuation, and therefore more shear stress on the heat transfer surface; therefore, the removed mass rate would be increased with time. This increase could be justified by considering an increase in flow rate would cause more heating of the surface element. The increase in flow rate contributes to the rise of mass removal and hence a reduction of $x_{f,t}$ and $R_{f,t}$. On the other hand and according to Eq. (20), an increase in the amplitude would cause the inlet fluid velocity to increase. Therefore, the surface temperature would increase and the $x_{f,t}$ of this salt ($CaSO_4$) on the cold surface decreases.

The decrease of the deposition mass rate per unit time could be

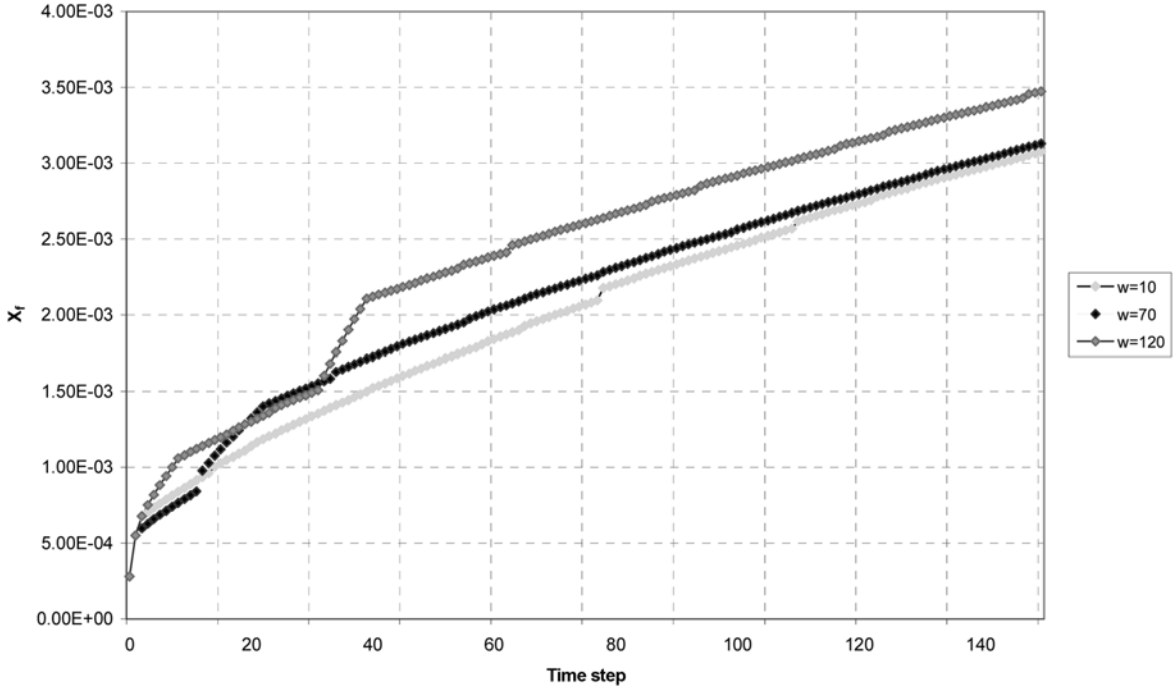

Fig. 7. The effects of variation of angular frequencies on fouling thickness.

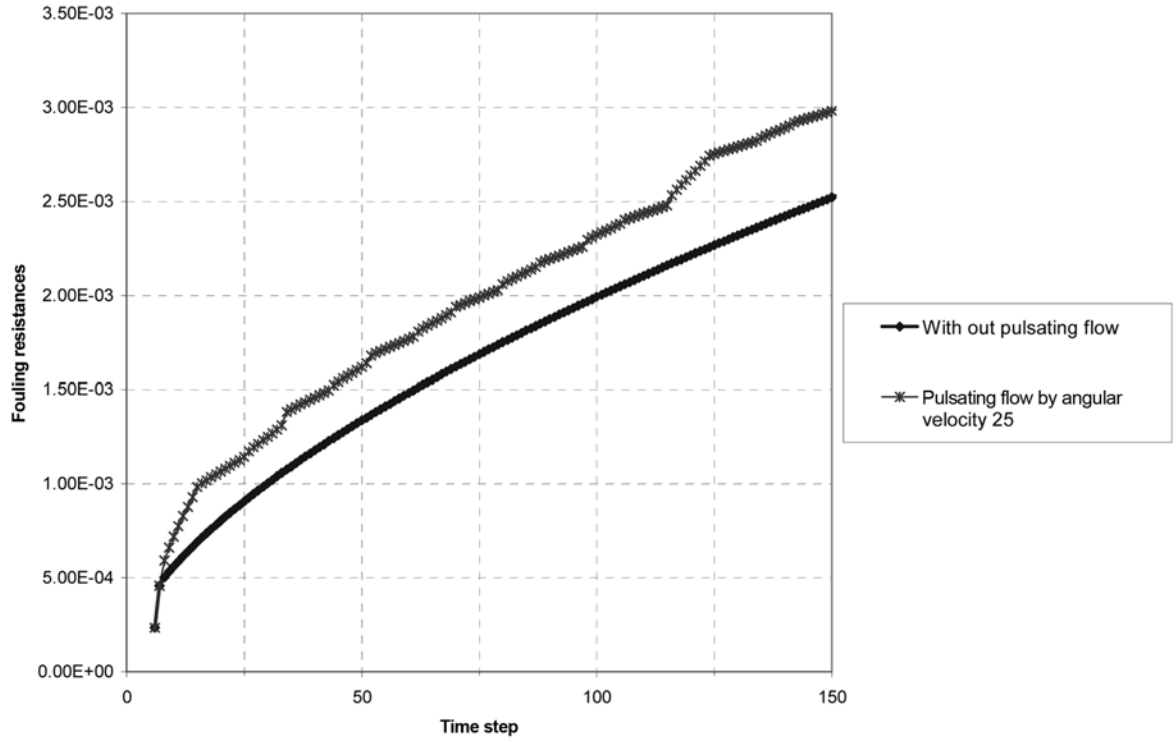

Fig. 8. Fouling resistance with and without pulsating flow.

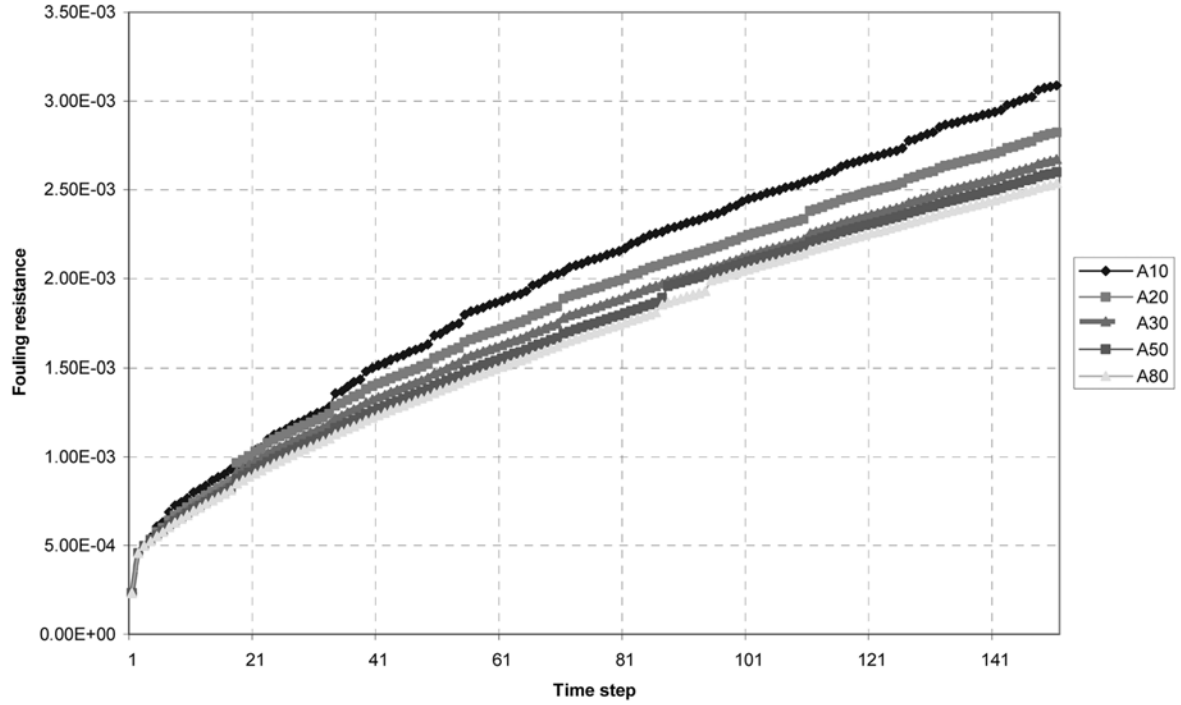

Fig. 9. The effect of oscillation amplitude on fouling resistance.

justified by the decrease in the surface temperature of the fouling layer. This occurs at higher fluid velocities and hence the heat transfer would be enhanced. The increase of mass transfer coefficient, owing to the flow rate acceleration, is relatively small. Therefore, it does not considerably affect the computation of the deposition mass rate.

CONCLUSION

Heat exchangers are typically overdesigned by 70-80% to account for unreliable design procedures and operational problems and out of this 30-50% is attributed to fouling alone. So if we could predict

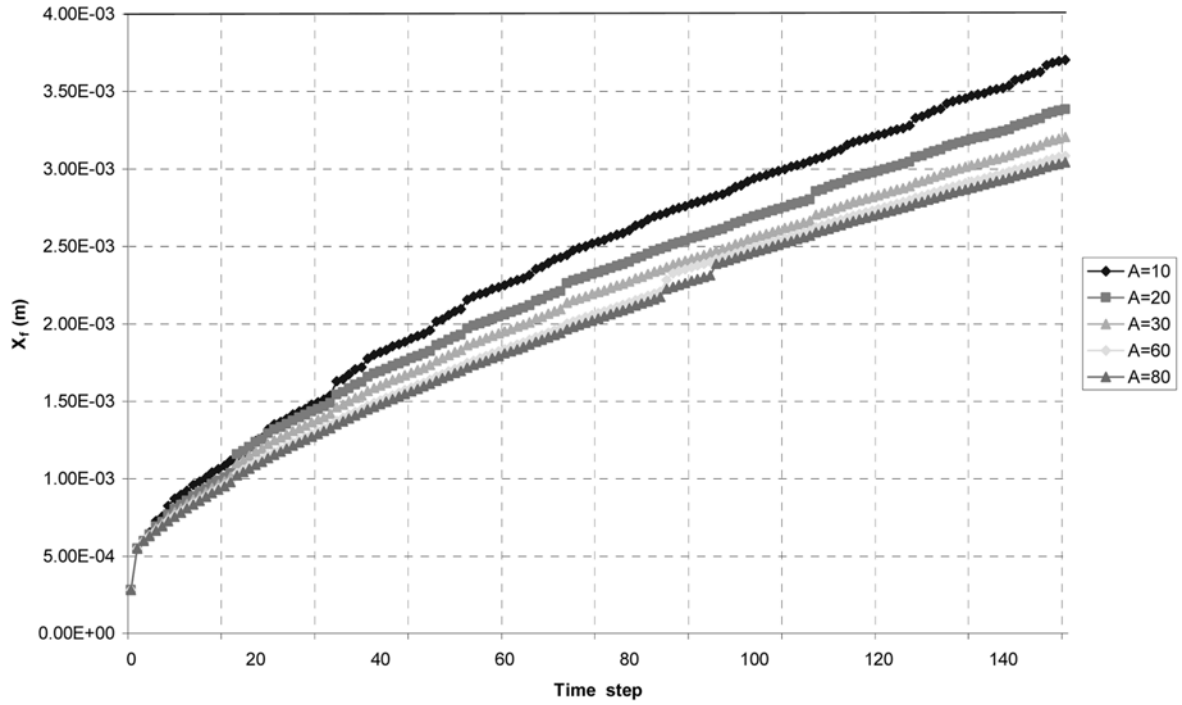

Fig. 10. The effect of oscillation amplitude on fouling thickness.

the thickness of fouling layer by passing time, it would significantly reduce the operation costs. The objective of this investigation was focused on the prediction of fouling thickness and fouling resistance of $CaSO_4$ which is one of the most important salts in water. The two-dimensional convective heat transfer calculations were performed at low and moderate Reynolds number values with an incoming pulsating flow. The sinusoidal pulsating flow was introduced with varying frequency and amplitude. Varying the amplitude and frequency of the pulsating flow will introduce instability to the flow and force the flow to become unsteady with the formation of vortices. These vortices play an important role in energy transport [20]. The heat transfer rate is enhanced for the high pulsating frequency of the range f=(1.59, 12.73 Hz) at A=80. The fouling resistance is directly decreased for the rise of the amplitude because of a higher free stream velocity.

Increasing the pulsating amplitude leads to a secondary shear layer, with a formation of pairing, merging and shedding of vortices in the layer again. The temperature is concentrated downstream and close to the wall because of this effect. The present investigation provides valuable insight into the dynamics and the mechanism of heat transfer process. Further investigation in the fouling of the flow, which is linked to the heat transfer, needs to be studied in more detail, especially for three-dimensional flow.

ACKNOWLEDGMENTS

The financial support provided by the Petrochemical Research and Development Company is gratefully acknowledged.

NOMENCLATURE

c_F : concentration of salt solution [kg/m^3]
c_s : saturation concentration [kg/m^3]
c_f : concentration in the vicinity of the fouling layer [kg/m^3]
$\dot{m}$: total mass rate [kg/m^2 s]
$\dot{m}_d$: deposition mass rate [kg/m^2 s]
$\dot{m}_r$: removal mass rate [kg/m^2 s]
$\dot{q}$: heat flux [W/m^2]
R_f : fouling resistance [W/m^2 K]
T_f : temperature of fouling layer surface [K]
x_f : thickness of crystal layer [m]
ω : fluid velocity above the fouling layer [m/s]
λ_f : thermal conductivity of fouling layer [W/m k]
ε : dissipation rate of turbulent kinetic energy [m^2/s^3]

REFERENCES

1. A. Al-Haddad and N. Al-Binally, *International Journal of Heat and Fluid Flow*, **10**, 131 (1989).
2. P. P. Grassmann and M. Tuma, *International Journal of Heat and Mass Transfer*, **22**, 799 (1978).
3. X. Wang and N. Zhang, *Journal of Heat and Mass Transfer*, **48**, 3957 (2005).
4. H. Gomaa and A. M. Al Taweel, *Chem. Eng. J.*, **102**, 71 (2004).
5. M. R. Mackley and P. Stonestreet, *Chem. Eng. Sci.*, **50**, 2211 (1995).
6. C. R. Brunold, J. C. B. Hunns, M. R. Mackley and J. W. Thompson, *Chem. Eng. Sci.*, **44**, 1227(1989).
7. T. Howes, M. R. Mackely and E. P. L. Roberts, *Chem. Eng. Sci.*, **46**, 1669 (1991).
8. S. A. Gbadebo, A. M. Said and M. A. Habib, *Journal of Heat and Mass Transfer*, **35**, 377 (1999).
9. V. Pérez-Herranz, J. L. Guiñón and J. Garca-Antón, *Chem. Eng. Sci.*, **54**, 1667 (1999).
10. R. C. Martinelli, L. M. K. Boelter, E. B. Weinberg and S. Yakahi,

Transactions of the American Society of Mechanical Engineers, **65**, 789 (1943).
11. Z. X. Mao and T. J. Hanratty, *Experiments in Fluids*, **2**, 129 (1985).
12. Z. X. Mao and T. J. Hanratty, *Journal of Fluid Mechanics*, **170**, 545 (1986).
13. A. Velazquez, J. R. Arias and J. L. Montanes, *International Journal of Heat and Mass Transfer*, **52**, 647 (2009).
14. F. Brahim, W. Augustin and M. Bohnet, *International Journal of Thermal Sciences*, **42**, 323 (2003).
15. FLUENT 6.1, Users's Guide.
16. J. Lammers, Diss. TU Berlin (1972).
17. M. Bohnet, W. Augustin and H. Hirsch, *Influence of fouling layer shear strength on removal*, United Engineering Foundation and Begell House, New York (1997).
18. F. Brahim, W. Augustin and M. Bohnet, *ECI Conference on heat exchanger fouling and cleaning: Fundamentals and applications*, **17** (2004).
19. Y. Chen and J. Zhao, *ICEBO2006, Shenzhen, China HVAC technologies for energy efficiency*, IV-6-3 (2006).
20. A. Suksangpanomrung, S. Chungpaibulpatana and P. Promvonge, *International Communications in Heat and Mass Transfer*, **34**, 829 (2007).